Available online at www.sciencedirect.com
SCIENCE DIRECT®
Catalysis Today 87 (2003) 43–50
CATALYSIS TODAY
www.elsevier.com/locate/cattod

# Quantum-chemical study on the supported precious metal catalyst

Changho Jung [a], Yuki Ito [a], Akira Endou [a], Momoji Kubo [a], Akira Imamura [b], Parasuraman Selvam [a], Akira Miyamoto [a,c,*]

[a] *Department of Applied Chemistry, Graduate School of Engineering, Tohoku University, Aoba-yama 07, Sendai 980-8579, Japan*
[b] *Department of Mathematics, Faculty of Engineering, Hiroshima Kokusai Gakuin University, 6-20-1 Nakano, Aki-ku, Hiroshima 739-0321, Japan*
[c] *New Industry Creation Hatchery Center, Tohoku University, Aoba-yama 10, Sendai 980-8579, Japan*

**Abstract**

In this study, quantum-chemical calculations were performed on the interface characteristics of certain precious metal containing zirconia catalysts, viz., $M/ZrO_2$; M = Rh, Pd or Pt. Using periodic density functional theory method, we were able to show that the Pd-supported zirconia catalyst ($Pd/ZrO_2$) has outstanding performance for NO activation. However, it was noted that this catalyst is thermodynamically less stable than the analogous $Pt/ZrO_2$ system. In addition, using accelerated quantum-chemical molecular dynamics method, we also clarified that the free Pt particle has completely negative surface charge while particle supported on the $ZrO_2$ surface showed different surface density states.


*Keywords:* Zirconia; Quantum-chemical calculation; Precious metal catalyst

## 1. Introduction

Precious metals such as Rh, Pd and Pt are one of the essential ingredients for the so-called three-way automotive exhaust catalyst, which can simultaneously decrease the amount of the pollutants, viz., CO, HCs and $NO_x$. However, a uniform dispersion of the metal particles is necessary for the enhancement of the catalytic activity as well as for the reduction in the catalyst cost. Hence, various metal oxide supports have been utilized for the preparation of well-dispersed supported metal catalysts. In this regard, it is noteworthy here that, in recent years, zirconia ($ZrO_2$) has been increasingly used for a variety of applications including catalyst, catalyst support, fuel cell, automotive gas sensor, etc. [1–4]. The tailored physico-chemical properties of zirconia including structure, redox, and acid–base characteristics make it as an attractive catalyst and catalyst support for a number of reactions [1,3,5–7]. Zirconia exhibits three well-defined polymorphs, the monoclinic (m), tetragonal (t) and cubic (c) phases; it has also been shown that a high-pressure orthorhombic form exists. The monoclinic phase [8–10] is stable up to 1400 K where it transforms to the tetragonal phase [11,12], which is stable up to 1570 K while the cubic phase [13,14] exists up to the melting point of 2980 K [8–14]. However, the cubic phase can be stabilized by the addition of divalent cations such as $Ca^{2+}$, $Mg^{2+}$

* Corresponding author. Tel.: +81-22-217-7233; fax: +81-22-217-7235.
*E-mail address:* miyamoto@aki.che.tohoku.ac.jp (A. Miyamoto).

0920-5861/$ – see front matter © 2003 Elsevier B.V. All rights reserved.
doi:10.1016/j.cattod.2003.09.013

or $Y^{3+}$. The stabilized zirconia has been extensively studied both theoretically and experimentally due to its wide technological applications [15,16]. Among the numerous precious metal supported catalyst systems, e.g., $Pt/ZrO_2$, $Pt/TiO_2$, $Pt/Al_2O_3$, etc., the metal supported zirconia finds special attention owing the stability in wide temperature range, and that the latter two are deactivated under the same experimental conditions [17].

At this juncture, it is, however, important to mention here that only very few theoretical studies have been performed on the precious metal/$ZrO_2$ catalysts [18]. On the other hand, in recent years, computational methods have become a powerful research tool for understanding the chemical reactions. For example, methods based on quantum-chemical theory provide information at atomic/molecular level. In particular, the density functional theory (DFT) calculations provide accurate energetic and density state of materials including heavy metals. In this investigation, we employ periodic DFT calculations to study the interface properties of precious metal supported zirconia catalyst system ($M/ZrO_2$; M = Rh, Pd or Pt). On the other hand, the DFT methods demand huge computational costs, and hence only a small model (∼30–50 atoms; much smaller number for transition metals) can be simulated. In this regard, recently, we have successfully developed a novel quantum-chemical molecular dynamics program 'Colors' [19–23], which allows for the determination of important properties of molecules and molecular systems with large number of atoms. Further, this program is over 5000 times faster than the regular first principles molecular dynamics programs, and can therefore effectively simulate the chemical reaction dynamics by considering the electronic state of large simulation model systems. In this paper, we present the results on the activation NO over Rh, Pd and Pt supported $ZrO_2$ catalyst systems using both periodic density functional, and accelerated quantum-chemical molecular dynamics methods.

## 2. Method

### 2.1. Periodic density functional method

Periodic DFT calculations were performed by solving the Kohn–Sham equations self-consistently [24] as implemented in DMol3 software [25]. The one-electron Schrödinger equations were solved at $K = 0$ wave-vector point of the Brillouin-zone. In order to reduce a computational cost, all core electrons were represented by effective core pseudopotentials (ECP) [25]. Basis sets are represented by the numerical type atomic orbitals, and in this study double numerical with polarization (DNP) basis sets were employed. Vosk–Wilk–Nusair (VWN) [26] local correlation functional was used in order to optimize geometries. More accurate generalized gradient approximation (GGA) in terms of Perdew–Wang functional [27] was also used and the results are compared with those obtained by VWN. For the geometry optimization, BFGS algorithm [25] was employed. The self-consistent field (SCF) convergence criterion was set to $10^{-5}$ ha, while the gradient convergence was set to $10^{-3}$ ha/Bohr.

### 2.2. Quantum-chemical molecular dynamics method

The tight-binding quantum-chemical molecular dynamics calculations were performed using our originally developed "Colors" code [9–11]. In this program, the total energy and force for each atom are expressed by Eqs. (1) and (2), respectively.

$$E = \sum_{i=1}^{n} \frac{m_i v_i^2}{2} + \sum_{k=1}^{\mathrm{occ}} \varepsilon_k + \sum_{i>j} \sum \frac{Z_i Z_j e^2}{R_{ij}} + \sum_{i>j} \sum E_{\mathrm{rep}}(R_{ij}) \quad (1)$$

$$F_i = \sum_{j\neq i}^{n} \sum_{k=1}^{\mathrm{occ}} C_k^T \left(\frac{\partial H}{\partial R_{ij}}\right) C_k + \sum_{j\neq i}^{n} \sum_{k=1}^{\mathrm{occ}} \varepsilon_k C_k^T \left(\frac{\partial S}{\partial R_{ij}}\right) C_k - \sum_{j\neq i} \frac{Z_i Z_j e^2}{R_{ij}^2} + \sum_{j\neq i} \frac{\partial E_{\mathrm{rep}}(R_{ij})}{\partial R_{ij}} \quad (2)$$

where $Z_i$ is the atomic charge, $e$ the elementary electric charge, and $r_{ij}$ the interaction distance. The first term refers to the kinetic energy, the second term is the summation of the eigenvalues of all occupied orbitals calculated by the tight-binding calculation, and the third term represents the Coulombic interaction. The last term corresponds to the short-range exchange

repulsion energy. The short-range exchange repulsion term, $E_{rep}(R_{ij})$ is represented by the following equation:

$$E_{rep}(R_{ij}) = b_{ij} \exp\left[\frac{a_{ij} - r_{ij}}{b_{ij}}\right] \quad (3)$$

Here, the parameters $a$ and $b$ represent the size and stiffness, respectively.

### 2.3. First principles parameterization

In a similar way to the previous tight-binding quantum-chemical molecular dynamics method, we used various parameters in "Colors", viz., the valence state ionization potential (VSIP) of atomic orbital $i$ ($I_i = -H_{ii}$) and the Slater exponent of atomic orbital $i$ ($\zeta_i$). These parameters were determined by the first principles density functional calculations for various charges and spin states of the atoms. On the basis of the improvement in the Wolfsberg–Helmholz formula by Anderson [28] and Calzaferri et al. [29], we used the following expression for $H_{rs}$:

$$H_{rs} = \tfrac{1}{2} K_{rs}(H_{rr} + H_{ss}) S_{rs} \quad (4)$$

$$K_{rs} = 1 + (\kappa_{rs} + \Delta^2 - \Delta^4 \kappa_{rs}) \exp[-\delta_{rs}(R_{ij} - d_0)] \quad (5)$$

$$\Delta = \frac{H_{rr} - H_{ss}}{H_{rr} + H_{ss}} \quad (6)$$

where $\kappa$, $\delta$, and $d_0$ are parameters for the tight-binding Hamiltonian, and that $K_{rs}$, i.e., $\kappa_{rs}$ and $\delta_{rs}$ was determined for each pair of atomic orbitals to further improve the accuracy in the chemical bonding calculations. In the conventional tight-binding calculations, the total orbital energy is calculated by

$$E = \sum_{k=1}^{occ} \varepsilon_k \quad (7)$$

where $\varepsilon_k$ is the orbital energy. Taking into account the work by Anderson [28,30] and Anderson and Hoffman [31] to improve the accuracy in the total valence electron energy, we introduced the following term for individual atoms with a different charge on the basis of the total electron energy of the same atom with the same charge calculated by the DFT method ($E_{DFT}$):

$$\Delta E_i = E_{DFT} - \sum_{k=1}^{occ} \varepsilon_k \quad (8)$$

$\Delta E_i$ is calculated for every simulated atoms with different charges and used to correct the total orbital energy in the tight-binding calculations. The various structures during the molecular dynamics simulations were visualized using RYUGA program [32].

## 3. Results and discussion

### 3.1. DFT study of precious metal/$ZrO_2$ catalysts and their reactivity

In the present study, the (1 1 1) surface of monoclinic and cubic zirconia was employed for the calculation, as it is one of the stable surfaces for both these structures [33]. The cubic phase can, however, be stabled the addition of trivalent metal ions such as yttrium or calcium. Fig. 1 depicts the (1 1 1) surface of cubic and monoclinic structures consisting of 8 zirconium and 16 oxygen atoms. The simulation cell dimension of m-$ZrO_2$ (1 1 1) surface and c-$ZrO_2$ (1 1 1) surface were fixed to: $a = 7.32$ Å, $b = 7.44$ Å, $\alpha = \gamma = 90°$, $\beta = 114.7°$; $a = 6.21$ Å, $b = 7.17$ Å, $\alpha = \beta = \gamma = 90°$, respectively. A pseudo-vacuum was applied along the $c$-axis (~10 Å) on all of the surface models.

As shown in Fig. 2, at first, four atoms clusters of precious metals ($Pt_4$, $Pd_4$ and $Rh_4$) were deposited on the (1 1 1) surface of both c-$ZrO_2$ and m-$ZrO_2$ in such a way that each Pt atom is bonded to surface

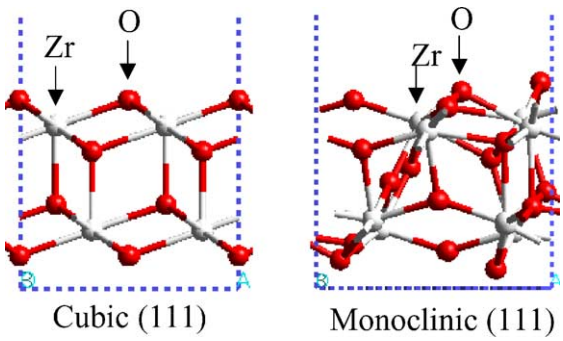


Fig. 1. Cubic and monoclinic $ZrO_2$ (1 1 1) surfaces.

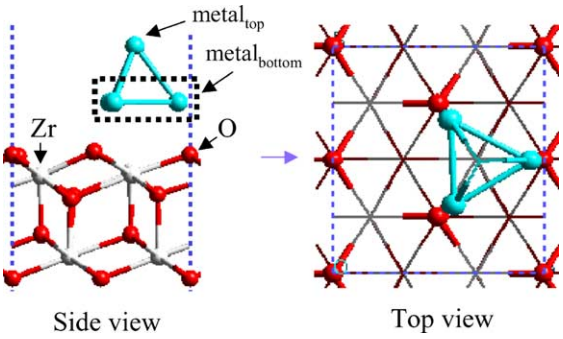


Fig. 2. Initial model for four (metal) atoms cluster on c-$ZrO_2$ (1 1 1) surface.

oxygen. However, geometry optimization, using VWN functional, results in the formation of three linear metal–oxygen (M–O) bonds on cubic (1 1 1) surface. On the other hand, two linear M–O bonds and one of the twofold M–O bond (one metal bonded with two surface oxygen) is noticed in the case of monoclinic (1 1 1) surface. This difference in the adsorbed structures could be attributed to the difference in surface oxygen–oxygen (O–O) distance. For example, in the case of cubic $ZrO_2$ (1 1 1), the O–O distance is 3.585 Å while for the monoclinic $ZrO_2$ (1 1 1) surface, four different O–O distance exists, i.e., 3.697, 3.214, 3.182 and 2.888 Å. Two surface oxygen atoms with 2.888 Å seem to be more suitable to make the twofold adsorption structure with the metal clusters.

Table 1 presents the optimized bond distances of metal–metal (M–M) and M–O. In this table, metal$_{bottom}$ indicates three metal atoms are bonded to the surface oxygen, while metal$_{top}$ means that another metal atom is located on top of the three metal (metal$_{bottom}$) atoms. We have also calculated the M–M distance for the isolated $M_4$ clusters and the values are 2.62, 2.59, and 2.46 Å for the $Pt_4$, $Pd_4$ and $Rh_4$, respectively. However, as can be seen from Table 1, for all the supported clusters, the metal$_{bottom}$–metal$_{bottom}$ distances are elongated while the metal$_{bottom}$–metal$_{top}$ distances are shortened. Such an effect is more pronounced in the case of cubic structure as the metal$_{bottom}$–oxygen$_{surface}$ distance, i.e., three linear metal$_{bottom}$–oxygen$_{surface}$ bonds, is much shorter as compared with the monoclinic surface where the twofold metal$_{bottom}$–oxygen$_{surface}$ bond has much lower influence on the metal$_{bottom}$–metal$_{top}$ distance. Further, it was also noticed that the rearrangement of the metal clusters occurred more significantly on the monoclinic surface.

Table 2 summarizes the adsorption energy and charge state of each metal clusters. As can be seen from this table that $Pt_4$ cluster shows much stronger interaction with cubic and monoclinic surface than the $Pd_4$ cluster, indicating that the $Pt_4/ZrO_2$ interface is energetically more stable than the corresponding $Pd_4/ZrO_2$ interface. On the other hand, the adsorbed metal clusters have positive charges, and the negative charges are transferred to the surface oxygen. Further, $Pd_4$ cluster shows much larger positive charge than $Pt_4$ cluster on $ZrO_2$ (1 1 1) surface. The very different charge transfer pattern and adsorption energy behavior of these metal clusters can be explained by considering the HOMO–LUMO levels of metal cluster on the $ZrO_2$ surface. Fig. 3 shows the calculated HOMO–LUMO levels of isolated $Pt_4$ and $Pd_4$ clusters as well as isolated c-$ZrO_2$ (1 1 1) surface. This figure reveals that the charge transfer of $Pd_4$ to c-$ZrO_2$ could occur much easily than that with $Pt_4$ to c-$ZrO_2$. Conversely, charge transfer of c-$ZrO_2$ (1 1 1) surface to $Pd_4$ has larger energetic barrier in comparison with c-$ZrO_2$ (1 1 1) surface to $Pt_4$. Thus, $Pd_4$

Table 1
Optimized structure of $M_4$ clusters on $ZrO_2$ (1 1 1) surface

| $ZrO_2$ phase | Metal cluster | Average distance of metal$_{bottom}$–metal$_{bottom}$ (Å) | Average distance of metal$_{bottom}$–metal$_{top}$ (Å) | Average distance of metal$_{bottom}$–oxygen$_{surface}$ (Å) |
|---|---|---|---|---|
| Monoclinic | $Pt_4$ | 2.742 | 2.568 | 2.076 |
| | $Pd_4$ | 2.687 | 2.553 | 2.124 |
| | $Rh_4$ | 2.553 | 2.448 | 2.107 |
| Cubic | $Pt_4$ | 2.632 | 2.546 | 2.039 |
| | $Pd_4$ | 2.632 | 2.546 | 2.039 |
| | $Rh_4$ | 2.503 | 2.446 | 2.031 |

Table 2
Adsorption energy and charge of $M_4$ clusters on $ZrO_2$ (1 1 1) surface

| $ZrO_2$ phase | Metal cluster | $E_{ads}^{PW91}$ (kcal/mol) | Average charge of cluster | Charge of $M_{bottom}$ | Charge of $M_{top}$ |
|---|---|---|---|---|---|
| Monoclinic | $Pt_4$ | −93.2 | +0.204 | +0.165 to −0.004 | −0.018 |
| | $Pd_4$ | −56.5 | +0.490 | +0.233 to +0.129 | −0.029 |
| | $Rh_4$ | −75.6 | +0.255 | +0.057 to +0.137 | −0.024 |
| Cubic | $Pt_4$ | −90.0 | +0.184 | +0.041 to +0.053 | −0.077 |
| | $Pd_4$ | −60.5 | +0.363 | +0.118 to +0.137 | −0.034 |
| | $Rh_4$ | −84.1 | +0.194 | +0.062 to +0.095 | −0.057 |

cluster has larger positive charge compared with $Pt_4$ cluster. Moreover, this result suggests that adsorption energy of the metal cluster is related not only to charge donation of metal cluster to $ZrO_2$ surface but also charge back-donation of $ZrO_2$ surface to metal cluster. In addition, clear charge polarization was observed for the supported metal clusters. Three metals bonded with $ZrO_2$ surface ($metal_{bottom}$) show positive charge while the metal non-bonded with $ZrO_2$ surface ($metal_{top}$) shows negative charge.

Fig. 4 shows the NO adsorption model of the precious metal (Pt or Pd) supported c-$ZrO_2$ (1 1 1) surface. In these calculations, the metal cluster/c-$ZrO_2$ was fixed for the geometry optimization of NO molecule. Table 3 gives the calculated properties of NO adsorption on $Pt_4$/c-$ZrO_2$ and $Pd_4$/c-$ZrO_2$ systems. It can be noticed from this table that the optimized NO bond length ($d_{NO}$) indicates a bridge and threefold site adsorption that makes longer NO bond length than the on-top site adsorption. The longer NO bond distance suggests a larger π-contribution between NO molecule and metal clusters. This π-interaction, however, weakens the NO bond because it increases the population on the NO 2π antibonding orbital. The NO molecular charge ($q_{NO}$) on $Pd_4$/$ZrO_2$

Table 3
No adsorption feature on metal/c-$ZrO_2$ catalyst

| Cluster | Site | $E_{ads}^{PW91}$ (kcal/mol) | $q_{NO}$ | $\Delta q$ of cluster | $d_{NO}$ (Å) |
|---|---|---|---|---|---|
| $Pt_4$ | On-top | −36.2 | −0.053 | +0.005 | 1.167 |
| | Bridge | −12.6 | −0.061 | −0.007 | 1.179 |
| | Threefold | −13.5 | −0.062 | +0.004 | 1.181 |
| $Pd_4$ | On-top | −41.1 | −0.109 | +0.106 | 1.164 |
| | Bridge | −42.0 | −0.261 | +0.260 | 1.200 |
| | Threefold | −25.1 | −0.265 | +0.285 | 1.215 |

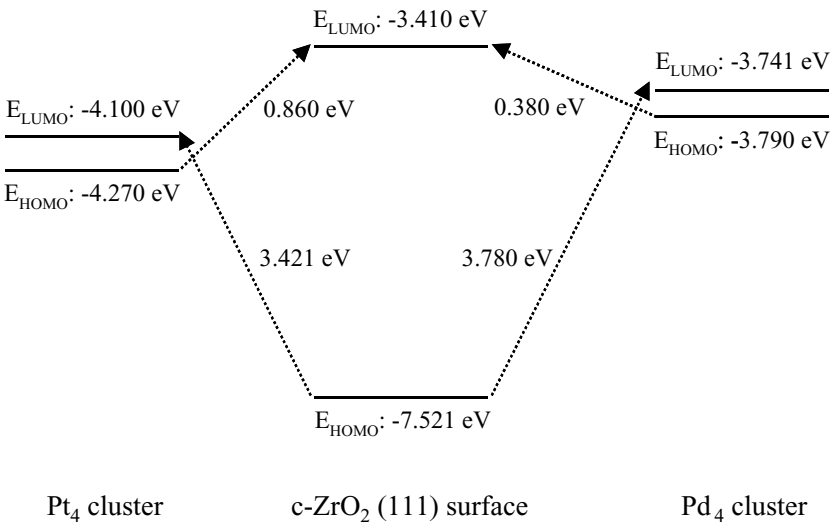


Fig. 3. HOMO–LUMO level of isolated $Pt_4$ and $Pd_4$ clusters as well as c-$ZrO_2$ (1 1 1) surface.

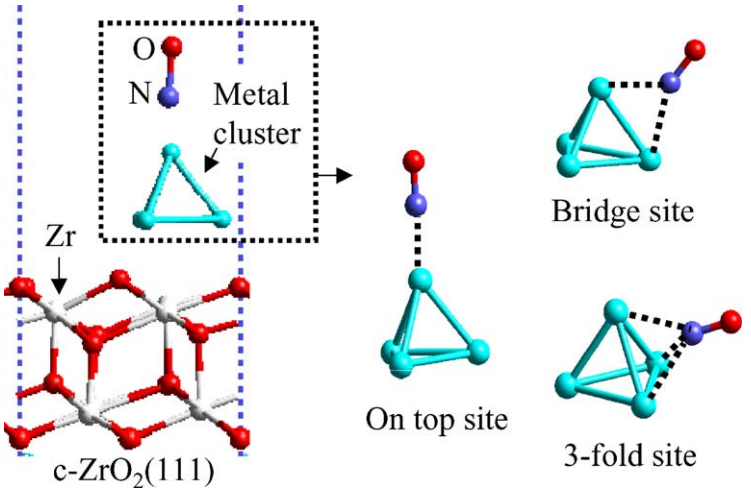


Fig. 4. NO adsorption site on $M_4$ cluster ($Pt_4$ and $Pd_4$) supported on c-$ZrO_2$ (1 1 1) surface.

is much larger than that on $Pt_4/ZrO_2$ in all of adsorption site. Moreover, $Pt_4$/c-$ZrO_2$ system shows clear site tendency of on-top site NO adsorption while $Pd_4/ZrO_2$ system shows considerably stronger adsorption energy on the bridge and threefold site compared with $Pt_4/ZrO_2$ system. This reveals that the Pd cluster is more suitable for the NO dissociation because bridge site and threefold site adsorption make longer NO bond distance with much larger $\pi$-contribution than on-top site adsorption. However, the $Pd_4$ cluster shows lower stability on the $ZrO_2$ (1 1 1) surface compared with $Pt_4$ cluster. These results indicate that the $Pd_4$/c-$ZrO_2$ could be a suitable catalyst as preventing Pd sintering on the $ZrO_2$ (1 1 1) surface. Thus, it can be deduced that the Pt/$ZrO_2$ catalyst could be used in a condition of higher temperature because of its higher energetic stability while the Pd/$ZrO_2$ catalyst is more suitable in lower temperature condition. In addition, NO adsorption makes a significant change of $Pd_4$ cluster charge ($\Delta q$ of cluster) in $Pd_4$/c-$ZrO_2$ system, while the $Pt_4$/c-$ZrO_2$ system shows almost same $Pt_4$ cluster charge during the NO adsorption.

### *3.2. Quantum-chemical molecular dynamics study on the small Pt particle and Pt/$ZrO_2$*

For the accelerated quantum-chemical molecular dynamics calculations, we selected two types of isolated Pt cluster models, i.e., $Pt_{13}$ and $Pt_{55}$. Fig. 5 illustrates the c-$ZrO_2$ (1 1 1) supported $Pt_{13}$ cluster. This c-$ZrO_2$ (1 1 1) surface include 24 atoms of zirconium and 48 oxygen atoms with a simulation cell dimension of $a = 10.76$ Å, $b = 12.42$ Å and $\alpha = \gamma = 90^\circ$. We already established original first principle parameterization for accelerated quantum-chemical molecular dynamics calculation [21–23], and same procedure was performed on this study. Table 4 shows the Pt cluster properties after geometrical relaxation by DFT method and our accelerated quantum-chemical molecular dynamics calculation. This result reveals that the 'Colors' code give us very accurate properties on $Pt_{13}$ cluster calculation compared with DFT method. Both of DFT and 'Colors' results also indicate that surface charge of the $Pt_{13}$ cluster is negative. In the case of the latter calculations, the $Pt_{55}$ cluster has $-0.120$ of surface Pt atomic charge while the $Pt_{13}$ cluster shows $-0.017$ of surface Pt atomic charge. This result suggests that the negative surface charge could be related

Table 4
Optimized free Pt particle properties

| | $Pt_{13}$ (DFT) | $Pt_{13}$ (Colors) | $Pt_{55}$ (Colors) |
|---|---|---|---|
| Binding energy (eV) | −53.2 | −53.5 | −399.2 |
| Surface Pt charge | −0.012 | −0.017 | −0.120 |
| Surface Pt–Pt length (Å) | 2.623 | 2.620 | 2.626 |

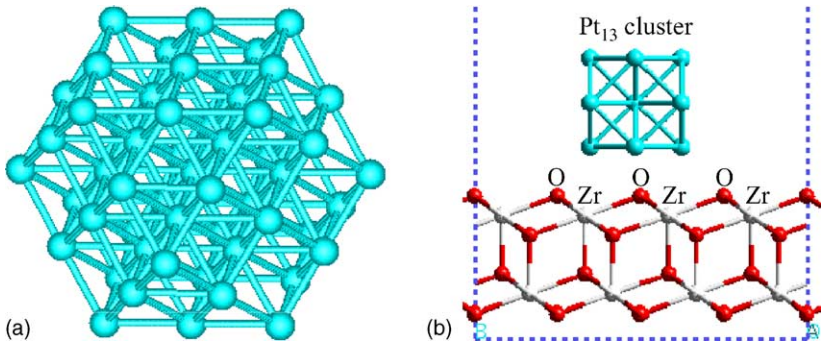


Fig. 5. (a) Isolated $Pt_{55}$ cluster, and (b) supported $Pt_{13}$ cluster on c-$ZrO_2$ (1 1 1) surface.

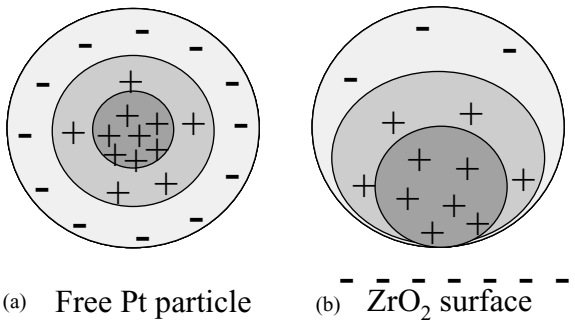


Fig. 6. Concept diagram for the charge distribution of: (a) free Pt particle, and (b) Pt particle on c-$ZrO_2$ (1 1 1) surface.

to the metal particle size. This charge transfer in Pt particles has a tendency of negative surface charge, while the inner atoms of particle have positive charge. In addition, the surface Pt–Pt bond length is almost the same on both $Pt_{13}$ and $Pt_{55}$ clusters after geometry relaxation. However, $Pt_{13}$ cluster on cubic $ZrO_2$ (1 1 1) surface shows more complex charge distribution, which can be separated to particle properties of Pt and effects from $ZrO_2$ support. This supported Pt particle has positive total charge, especially Pt atoms bonded with $ZrO_2$ surface show larger positive charge while other Pt atoms have almost neutral charge or neglect negative charge. Fig. 6 shows a concept of Pt particle charge distribution. Accordingly, we suggest that supported metal particle has variable surface density state, and that the very different surface density state could be related to very different activity of adsorbate molecules.

## 4. Conclusion

We performed quantum-chemical calculations on precious metal/$ZrO_2$ catalyst systems. Using DFT method, we clarified that the Pd/$ZrO_2$ catalyst has exceptional performance on the NO activation, while the Pd/$ZrO_2$ catalyst is thermodynamically unstable as compared with Pt/$ZrO_2$ catalyst. In addition, using accelerated quantum-chemical molecular dynamics method, we demonstrated that the free Pt particle has completely negative surface charge, and hence the particle shows different surface density states on the $ZrO_2$.

## References

[1] R. Srinivasan, B.H. Davis, Catal. Lett. 14 (1992) 165.
[2] S.C. Su, A.T. Bell, J. Phys. Chem. B 102 (1998) 7000.
[3] Z. Dang, B.G. Anderson, Y. Amenomiya, B.A. Morrow, J. Phys. Chem. 99 (1995) 14437.
[4] J.M. Miller, L.J. Lakshmi, J. Phys. Chem. B 102 (1995) 6465.
[5] K. Tanabe, Mater. Chem. Phys. 13 (1985) 347.
[6] R. Srinivasan, D. Taulbee, B.H. Davis, Catal. Lett. 9 (1991) 1.
[7] K. Tanabe, M. Misono, Y. Ono, H. Hattori, Stud. Surf. Sci. Catal. 51 (1989) 1.
[8] J. Adam, M.D. Rogers, Acta Crystallogr. 12 (1959) 951.
[9] J.D. McCullough, K.N. Trueblood, Acta Crystallogr. 12 (1959) 507.
[10] D.K. Smith, H.W. Newkirk, Acta Crystallogr. 18 (1965) 983.
[11] C.J. Howard, R.J. Hill, B.E. Reichert, Acta Crystallogr. B 44 (1988) 116.
[12] G. Teufer, Acta Crystallogr. 15 (1962) 1187.
[13] P. Aldebert, J.P. Traverse, J. Am. Ceram. Soc. 68 (1985) 34.
[14] R.J. Ackermann, S.P. Garg, E.G. Rauth, J. Am. Ceram. Soc. 60 (1977) 341.

[15] E.V. Stefanovich, A.L. Shluger, C.R.A. Catlow, Phys. Rev. B 49 (17) (1994) 11560.
[16] G. Stapper, M. Bernasconi, N. Nicoloso, M. Parrinello, Phys. Rev. B 59 (1999) 797.
[17] J.H. Bitter, K. Seshan, J.A. Lercher, J. Catal. 171 (1997) 279; J.H. Bitter, K. Seshan, J.A. Lercher, J. Catal. 176 (1998) 93; J.H. Bitter, K. Seshan, J.A. Lercher, J. Catal. 183 (1999) 336.
[18] M. Alfredsson, C.R.A. Catlow, Phys. Chem. Chem. Phys. 3 (2001) 4129.
[19] H. Takaba, A. Endou, A. Yamada, M. Kubo, K. Teraishi, K.G. Nakamura, K. Ishioka, M. Kitajima, A. Miyamoto, Jpn. J. Appl. Phys. 39 (2000) 2744.
[20] Y. Inaba, T. Onozu, S. Takami, M. Kubo, A. Miyamoto, A. Imamura, Jpn. J. Appl. Phys. 40 (2001) 2991.
[21] T. Yokosuka, H. Kurokawa, S. Takami, M. Kubo, A. Miyamoto, A. Imamura, Jpn. J. Appl. Phys. 41 (2002) 2410.
[22] M. Elanany, P. Selvam, T. Yokosuka, S. Takami, M. Kubo, A. Imamura, A. Miyamoto, J. Phys. Chem. B 107 (2003) 1518.
[23] Y. Luo, P. Selvam, Y. Ito, S. Takami, M. Kubo, A. Imamura, A. Miyamoto, Organometallics 22 (2003) 2181.
[24] W. Kohn, L.J. Sham, J. Phys. Rev. A 140 (1965) 1133.
[25] DMol3, Version 4.0, Accelrys, 1999.
[26] S.H. Vosk, L. Wilk, M. Nusair, Can. J. Phys. 58 (1980) 1200.
[27] J.P. Perdew, J.A. Chevary, S.H. Vosko, K.A. Jackson, M.R. Pederson, D.J. Singh, C. Fiolhais, Phys. Rev. B 46 (1992) 6671.
[28] A.B. Anderson, J. Chem. Phys. 62 (1975) 1187.
[29] G. Calzaferri, L. Forss, I. Kamber, J. Phys. Chem. 93 (1989) 5366.
[30] A.B. Anderson, J. Chem. Phys. 60 (1974) 2477.
[31] A.B. Anderson, R. Hoffman, J. Chem. Phys. 60 (1974) 4271.
[32] R. Miura, H. Yamano, R. Yamauchi, M. Katagiri, M. Kubo, R. Vetrivel, A. Miyamoto, Catal. Today 23 (1995) 409.
[33] S. Gennard, F. Cora, C. Richard, C.R.A. Catlow, J. Phys. Chem. B 103 (1999) 10158.